Batteries & Supercaps

Chemistry Europe
European Chemical Societies Publishing

Batteries & Supercaps

RESEARCH ARTICLE OPEN ACCESS

A Fluoropolymer-Based Gel Polymer Electrolyte Crosslinked by $NaBH_4$ for Application in Room-Temperature Sodium Batteries

Litwin Jacob[1,2] | Chinmaya Mirle[1,2] | Ziyuan Lyu[2,3,4] | Dominic Bresser[2,3,4,5] | Alexander J. C. Kuehne[1,2]

[1]Institute of Organic and Macromolecular Chemistry, Ulm University, Ulm, Germany | [2]CELEST Green Energy Lab Ulm, Ulm University, Ulm, Germany | [3]Helmholtz Institute Ulm for Electrochemical Energy Storage (HIU), Ulm, Germany | [4]Karlsruhe Institute of Technology (KIT), Karlsruhe, Germany | [5]Ulm University, Ulm, Germany

Correspondence: Alexander J. C. Kuehne (alexander.kuehne@uni-ulm.de)

Received: 24 March 2026 | **Revised:** 14 July 2026 | **Accepted:** 3 August 2026

Keywords: crosslinked gel polymer electrolyte | cycling stability | ionic conductivity | near-single-ion conduction | sodium metal battery

ABSTRACT

Rechargeable sodium-metal batteries are attractive for large-scale energy storage due to the high abundance and low cost of sodium. However, their development is hindered by the limited availability of electrolytes that simultaneously provide high ionic conductivity, high Na metal compatibility, and suppressed anion mobility. Here, we report a chemically simple gel polymer electrolyte (GPE) based on a commercially available hydroxyl-terminated fluoropolymer, in which a borate-mediated network is generated in situ using sodium borohydride as a low-cost crosslinking agent. The resulting GPE exhibits excellent Na^+ ionic conductivity up to 1.6×10^{-3} S cm^{-1} at 30 °C and near single-ion conduction (Na^+ ion transference number up to ~0.84). Galvanostatic cycling of a symmetric Na||Na cell using glass fiber-supported GPE exhibits stable performance over 750 cycles, demonstrating excellent GPE compatibility with Na metal. A coin cell assembled from an Na anode and a $Na_3V_2(PO_4)_3$/C cathode with this GPE exhibits an exceptional cycling performance with over 2000 charge–discharge cycles within the voltage range from 1 to 2 V.

1 | Introduction

The natural abundance and widespread distribution of sodium (Na) in the earth's crust and oceans make sodium-metal batteries (SMBs) an appealing alternative to lithium-ion batteries for future large-scale applications [1, 2]. Na has a high theoretical specific capacity of 1165 mAh g^{-1} and a low redox potential of −2.71 V versus the standard hydrogen electrode [3]. Accordingly, the potential use of Na as a metallic anode in SMBs significantly increases the overall battery capacity, voltage, and energy density compared to classic sodium-ion batteries, where both electrodes are just host materials for the Na ions [4, 5].

However, a number of issues remain in SMBs that must be resolved before they can be utilized in practical applications [6, 7]. The main challenge remains in finding a suitable electrolyte that is compatible with the reactive Na-metal electrode. Current challenges with the presently available electrolyte systems include side reactions and the formation of unstable or passivating interphases, compromising the cycling stability of the battery cell [8]. Moreover, Na tends to deposit unevenly, causing dendrite formation, which eventually could cause shorting and failure of the SMBs [3]. Additionally, state-of-the-art liquid electrolytes are often flammable and volatile, and they can leak from a failing or expanding SMB, raising safety concerns [9]. One approach to address the above-described shortcomings is the use of solid-state electrolytes (SSEs), for instance, solid inorganic Na superionic conductors (NASICON) or polymer-based electrolytes [10–12]. In comparison with classic liquid electrolytes, SSEs offer a number of benefits, including good thermal stability, as well as

reduced electrolyte volatility and leakage (for improved safety) [11]. Despite having a high sodium-ion transference number (~1) and high ionic conductivity ($\geq 10^{-3}$ S cm^{-1} at ambient conditions), inorganic solid electrolytes suffer from their rigid ceramic nature, leading to poor interfacial contact. Furthermore, their commercial use is hampered by challenges in synthesis and difficult to control thickness variations together with complicated device integration procedures [13]. By contrast, polymer-based electrolytes offer great potential because of their facile processability, exceptionally low electrode resistance, and good flexibility [14, 15]. However, the majority of the polymer-based electrolytes lacks sufficient ionic conductivity ($<10^{-6}$ S cm^{-1} at 25 °C) at ambient conditions and exhibits relatively low transference numbers (~0.3) [16, 17].

By contrast, gel polymer electrolytes (GPEs) combine the properties of solid, polymer, and liquid electrolytes, with acceptable mechanical strength, high thermal stability, and good interface properties, together with superior ionic conductivity of 10^{-4}–10^{-3} S cm^{-1} at room temperature [18, 19]. GPEs are polymer networks that are swollen with a liquid electrolyte. Within the gel network, the liquid is bound and therefore not free-flowing. Recently, several GPEs have been identified as potential candidates for Na batteries due to their ability to stabilize the interface and reduce interfacial resistance between the electrodes and the electrolyte. One such system is a fluoroethylene carbonate-modified GPE, containing sodium bis(trifluoromethylsulfonyl)imide salt, which demonstrated excellent ionic conductivity of 3.8×10^{-3} S cm^{-1} at 25 °C and high cycling stability with 95% capacity retention at 5C after 1000 cycles [20]. Several composite GPEs (CGPEs) have also been explored, and they have shown to inhibit uneven deposition of sodium, preventing dendrite formation and improving the safety of SMBs [21, 22]. Despite these various advances, the presence of structurally and chemically incompatible interfaces between the organic polymer substrate and the inorganic components in CGPEs results in low ionic conductivity and ineffective Na^+ transport [23]. In most of the cases, the added inorganic fillers and plasticizers cause the GPEs to lose their mechanical properties because of the lack of structure-stabilizing interactions between the additives and the gel network. Moreover, the majority of reported gel electrolytes are "classic" dual-ion conducting systems with low cation transference numbers (<0.4), which leads to a steep ion concentration gradient near the electrode surfaces that strongly reduces the battery capacity and favors dendrite growth [24].

Several approaches have been explored to overcome the aforementioned difficulties, such as (i) the use of fluorinated solvents to generate a sodium fluoride NaF-rich stable solid electrolyte interphase (SEI) [25]. Moreover, (ii) additives have been admixed to the electrolyte to stabilize the interface and interphase [6, 26, 27], or (iii) an artificial SEI between the GPE and the Na-metal anode has been established [28]. (iv) The mechanical properties and (v) the ionic conductivity of the GPE have been tuned through crosslinking and variation of the crosslinking density [29, 30], and (vi) anions have been immobilized in the GPE to increase the transference number of the cation [31]. Among these, GPEs without inorganic additives or the use of an artificial SEI could avoid undesired side reactions, reduce production costs, and obviate complications during battery fabrication.

Despite these advances, electrolyte concepts that combine high cation transference numbers, interfacial compatibility with Na metal, and facile synthesis from commodity materials remain scarce. In particular, many reported high-performance GPEs rely on multistep polymer synthesis, expensive crosslinkers, or inorganic fillers that complicate processing and scale-up. Against this background, sodium borohydride ($NaBH_4$) represents an attractive yet underexplored building block for gel electrolytes, as it simultaneously provides sodium ions, boron-based coordination sites, and reductive stability toward alkali-metal anodes, while being inexpensive and industrially available.

In this study, we present a crosslinked GPE based on a commercially available fluoropolymer (Lumiflon LF9716, a fluoroethylene vinyl ether polyol containing high amounts of hydroxyl functionality with a hydroxyl value of 170 mg KOH/g polymer) that is crosslinked by $NaBH_4$ for use in ambient-temperature SMBs. A crosslinking reaction between the hydroxyl groups of the fluoropolymer and $NaBH_4$ in a suitable glyme solvent system results in GPEs with largely immobilized anions in the gel polymer network, complementing the high compatibility of glyme-type solvents with Na-metal anodes [32, 33]. The resulting GPE provides an excellent ionic conductivity of up to 1.6×10^{-3} S cm^{-1} at 30 °C and still 6.4×10^{-4} S cm^{-1} at −20 °C. Galvanostatic cycling of symmetric cells indicates very reversible Na plating and stripping. Moreover, a standard reference cell (Na|GPE|$Na_3V_2(PO_4)_3$/C (NVP/C)) delivers ultralong cycling stability for over 2000 charge–discharge cycles at 1C. This work opens up a promising electrolyte design strategy that can be modified to satisfy the requirements of SMBs.

2 | Results and Discussion

2.1 | Synthesis and Structural Characterization of GPE

To form our GPE, we employ a hydroxyl-terminated fluoropolymer (Lumiflon LF9716, M_n = 34,000 g mol^{-1}, 3.025 mmol OH-groups/g polymer) in dimethoxyethane (DME) together with $NaBH_4$ (2 M solution in triethylene glycol dimethyl ether (TREGDME)). The mixture of DME (boiling point (bp) 85 °C, melting point (mp) –69 °C, viscosity η = 0.46 cP at 25 °C, dielectric constant κ = 7.1) and TREGDME (bp 216 °C, mp –45 °C, η = 1.95 cP at 25 °C, κ = 7.5) is beneficial due to the low viscosity and melting point of DME and the high dielectric strength and boiling point of TREGDME [34, 35]. These solvents together have favorable effects on the Na^+ ion transport, as well as on the electrochemical and thermal stability [36]. TREGDME also offers good solubility for $NaBH_4$. Furthermore, the (C—F···H—C) halogen bond between the fluoropolymer and solvent molecules enhances the dispersibility and thermal stability of the resulting GPE [37]. In addition, the fluorinated segments in the fluoropolymer can support the formation of an SEI rich in fluorine containing organic components. This SEI stabilizes the metal anode and improves the cycling stability [38–41].

Borohydrides, being inherently strong reductants, are also compatible with metal anodes [42–44]. The degree of crosslinking and the mechanical properties of the GPE electrolyte are tuned by varying the concentration of $NaBH_4$ ($c(NaBH_4)$). During the

gelation process, the $[BH_4]^-$ species interact with the hydroxyl groups of the fluoropolymer, leading to the formation of boron–oxygen coordination motifs and a borate-mediated network, in which solvent molecules become confined (Figure 1a). To study the effects of crosslinking and $NaBH_4$ loading, we prepare several GPE samples by varying the $c(NaBH_4)$ (from 15 to 115 wt%) with respect to 110 mg of fluoropolymer. In a typical reaction, the total volume of the electrolyte is adjusted to 3 mL, and the volume of DME is varied depending on the volume of $NaBH_4$ solution in TREGDME required to form the GPE. For instance, mixing a solution of fluoropolymer (110 mg) in 2.2 mL DME and 0.8 mL of 2 M $NaBH_4$ in TREGDME results in a GPE containing 55 wt% (60.5 mg) of $NaBH_4$ (see the experimental section and Table S1 for more details). Mixing of the two components leads to slow gelation of the sample over 4–5 days (see Figure 1b). Electrolyte samples containing stoichiometric ($c(NaBH_4) \approx 3$ wt%) and substoichiometric amounts of the $NaBH_4$ crosslinker do not form gels. By contrast, the samples containing superstoichiometric concentrations of $NaBH_4$ form gels, and those with higher concentrations retain their gel nature even after several days in an open atmosphere (see Figure S1).

The resulting GPEs are studied using infrared spectroscopy (IR), solid-state ^{11}B NMR spectroscopy, X-ray diffraction (XRD), and differential scanning calorimetry (DSC). The pristine fluoropolymer exhibits absorbance by the hydroxyl groups between 3400 and 3500 cm^{-1} in the IR spectrum (see Figure 1d). Following the formation of the GPE with $NaBH_4$, the hydroxyl band vanishes, providing the first evidence for the consumption of OH groups in the formation of boron-centered crosslinks. The newly appearing IR signals in the GPE located between 1025 and 600 cm^{-1} can be attributed to these boron–oxygen bonds [45]. Unsurprisingly, the superstoichiometric application of $NaBH_4$ also provides a broad B—H stretching absorption between 2200 and 2400 cm^{-1}, indicating the presence of unreacted B—H moieties, for example, in the gel composition 55 wt% of $NaBH_4$ (see Figure 1e). Further more, to investigate the bond number of the boron-centered crosslinks, we employ solid-state proton decoupled ^{11}B NMR ($^{11}B\{^1H\}$) spectroscopy. The broad peaks at 3 and –11 ppm in the spectrum of the GPE further substantiates the formation of $B(OR)_4^-$ and $BH(OR)_3^-$ species, respectively, indicating that the boron anions are contributing to crosslinking (see Figure 1g) [46]. The above observations suggest that a distribution of boron

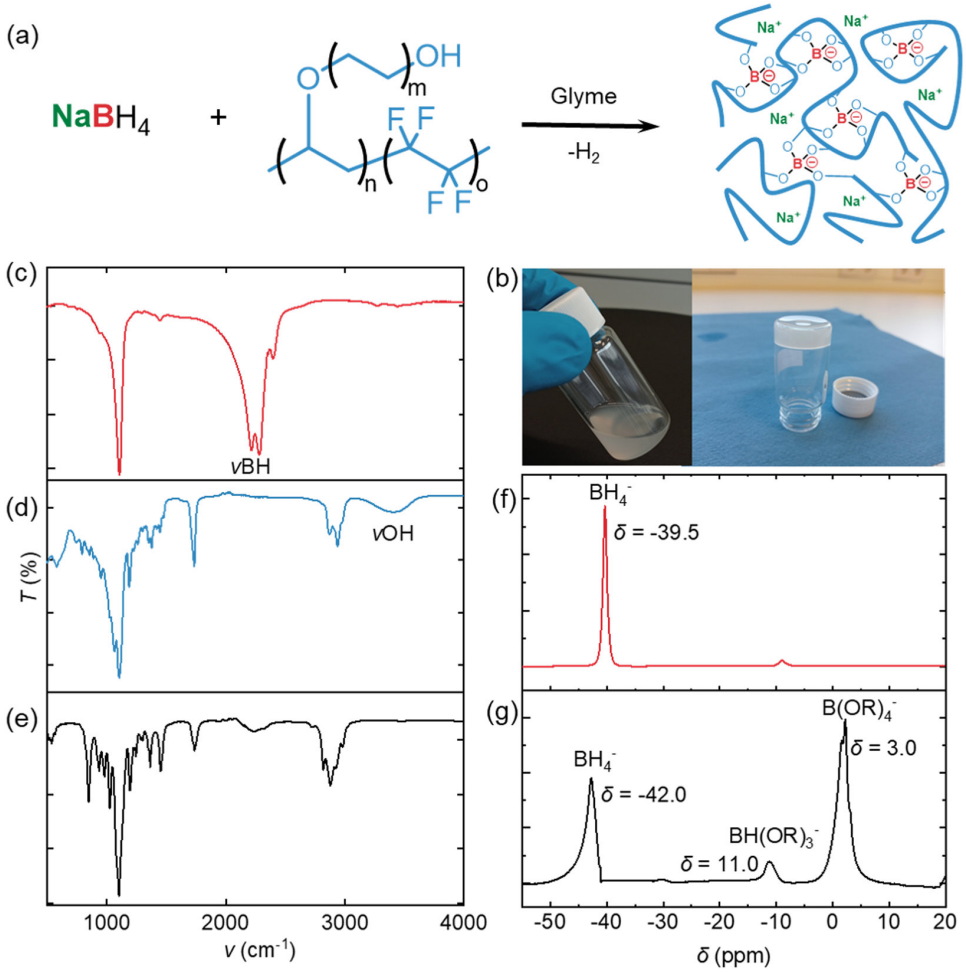

FIGURE 1 | (a) Components and synthesis of the GPE. The hydroxy groups of the Lumiflon fluoropolymer ($m = 1$–3, $n = 105$, $o = 200$–260) are crosslinked by borate anions. (b) Photographs of the electrolyte solution before and after gelation. The vial with the gel is turned upside down to indicate the gel state. (c) FTIR spectrum of the $NaBH_4$ powder with the characteristic BH stretching vibration. (d) FTIR spectrum of the Lumiflon fluoropolymer with the characteristic O—H stretching mode, and (e) showing the FTIR spectrum of the cured GPE containing 55 wt% $NaBH_4$ after drying in vacuum. The panels (f,g) show the proton decoupled solid-state ^{11}B NMR spectrum ($^{11}B\{^1H\}$) of $NaBH_4$ and the GPE containing 55 wt% $NaBH_4$ after drying in vacuum. Delta (δ) is the chemical shift in ppm.

coordination environments is present in the GPE, ranging from network-bound borate species (mono- to tetra-coordination of boron to the fluoropolymer via covalent B—O bond formation) to residual, noncovalently bound borohydride anions.

The formation of a GPE is further substantiated by the XRD pattern of our GPE sample, which does not feature any sharp reflections, corroborating an overall amorphous nature (see Figure S2). Here, $NaBH_4$ would be completely dissolved in the gel electrolyte, while the amorphous nature will be favorable for the Na^+ ion transport in the GPE. The DSC thermogram for the gel sample with 55 wt% $NaBH_4$ shows a clear endothermic event at $T \sim 77\,°C$ (see Figure S3). This can be attributed to a volume phase transition (VPT) of the crosslinked GPE. The endothermic event is reversible and when we heat a macroscopic sample of the gel, we observe cracking of the gel, which substantiates the contraction and release of solvents upon crossing of the VPT (see Figure S4).

Moreover, when we compare the NMR spectrum of pure $NaBH_4$ with that of the GPE, we observe a shift in the peak associated with the borohydride anions. This shift will arise from the existence of noncovalent bonding interactions in the GPE [47]. For instance, previous studies have shown the existence of noncovalent hydrogen bonding interaction of anions with acidic protons in a partially fluorinated polymeric network [48]. In a similar way, unreacted BH_4^- in the GPE is also expect to immobilize through noncovalent (B—H···H—C) charge-inverted hydrogen bonding interactions of unreacted BH_4^- with partially positively polarized hydrogen atoms in the fluoropolymer backbone. We perform correlative 2D ^1H—^1H NOESY NMR to test for this dipolar coupling using a solution of $NaBH_4$ in a small molecular fluoroether, as a structural analog of the fluoropolymer units (see Figure S5). The presence of cross peaks in the spectrum confirms the existence of intermolecular hydrogen bonding interaction between the two molecules. This substantiates our hypothesis of inherent ability of the GPE system to suppress the mobility of BH_4^- anions, favoring selective Na^+ ionic mobility.

All of the above investigation reveals that the GPE has a boron-centered fluoropolymer network structure at ambient temperature, with covalently and noncovalently bound boron species in the GPE network.

2.2 | Ionic Conductivity and Charge Transport

To investigate the charge transport, we used electrochemical impedance spectroscopy (EIS) to determine the ionic conductivity. We correlate the ionic conductivity (σ) with the temperature (T from −20 to +50 °C) and the concentration of the $NaBH_4$ ($c(NaBH_4)$ from 15 to 125 wt%). The ionic conductivity (σ) is derived from the bulk resistance (R_b), which is determined from the high-frequency intercept with the real axis in the Nyquist plot. This experiment reveals a general trend for the ionic conductivity: σ increases with both rising T and $c(NaBH_4)$ up to a certain limit, after which σ declines. For instance, at $T = 30\,°C$, as $c(NaBH_4)$ in the GPE increases from 15 to 105 wt%, the ionic conductivity of the gel also increases from $\sigma = 0.1 \times 10^{-3}\,S\,cm^{-1}$ to a maximum of $\sigma = 1.6 \times 10^{-3}\,S\,cm^{-1}$ (see Figure 2a). However, further increasing $c(NaBH_4)$ to 125 wt% leads to a decrease in ionic conductivity to $\sigma = 1.0 \times 10^{-3}\,S\,cm^{-1}$. A similar trend is observed with temperature, σ in the GPE rises sharply with increasing T from −20 °C to a maximum at 30 °C. By contrast, beyond $T = 30\,°C$, σ decreases (see Figure 2a).

The influence of the $NaBH_4$ concentration on the ionic conductivity of the GPEs is illustrated by the linear dependence of σ on $c(NaBH_4)$ at $T = 30\,°C$ (see Figure 2b). The ionic conductivity initially increases with increasing $c(NaBH_4)$ owing to the higher concentration of mobile charge carriers. A maximum conductivity is reached at moderate $NaBH_4$ concentrations, whereas further increasing the salt concentration ($c(NaBH_4) > 105$ wt%) results in a decrease in σ. This behavior has previously been attributed to enhanced contact ion pair formation, which reduces the number of free charge carriers and consequently limits ion mobility [49, 50]. A similar effect governs the temperature dependence of the ionic conductivity (see Figure 2a). Above 30 °C, σ decreases despite the increase in thermal energy because the solubility of $NaBH_4$ in the DME/TREGDME electrolyte decreases with increasing temperature. As the dielectric constant of the solvent mixture decreases upon heating [51], which leads to the formation of contact ion pairs and precipitation of $NaBH_4$ at elevated temperatures, as shown in Figure S6 [52]. Consistent with this behavior, fitting the conductivity data between 30 and 40 °C using the Arrhenius equation yields an apparent negative activation energy (E_a, see Figure S7). This anti-Arrhenius behavior arises because thermally induced ion association outweighs the beneficial effect of increased thermal energy on ionic mobility.

To directly verify this mechanism, the temperature-dependent solubility of $NaBH_4$ was determined by iodometric back-titration using the same DME/TREGDME solvent mixture (2.75:1) employed in the GPE containing 55 wt% of $NaBH_4$. The measurements reveal a pronounced decrease in $NaBH_4$ solubility with increasing temperature, from 0.80 M at room temperature to 0.48 M at 40 °C (see Figure S8). Although this thermally induced electrolyte precipitation limits operation at elevated temperatures, it also defines a clear operational window for the electrolyte at low and ambient temperatures. In this context, the reversible contact ion pair formation highlights an inherent connection between ionic conductivity and a thermally controlled phase transition in our GPE, which could be used as a universal and tunable safety mechanism against cell overheating.

The Na^+ cation transference number (t_{Na^+}) of an electrolyte represents the share of the ionic conductivity carried by the cation. Thus, t_{Na^+} is a crucial parameter for the eventual performance, describing the accumulation and depletion of ions at the polarized electrode||electrolyte interfaces during cell operation. We determined t_{Na^+} for selected GPEs with $c(NaBH_4) = 35$, 55, 75, and 95 wt%, using chronoamperometry coupled with EIS (see Figure 2c,d) [53, 54]. For this, we fabricated symmetric Na|GPE|Na cells. We prepare all the coin cells using in situ formed GPE on a glass fiber (GF) separator to enhance the mechanical properties (see the experimental section and Figure S10 for the preparation). It should be noted that the present study focuses on the electrochemical functionality of the GPE rather than its mechanical strength, which might deserve further optimization. EIS is conducted to determine the resistance R_0 before polarizing the cell by applying a sinusoidal voltage with an amplitude of 30 mV, (see Figure 2c (inset)). The measured R_0

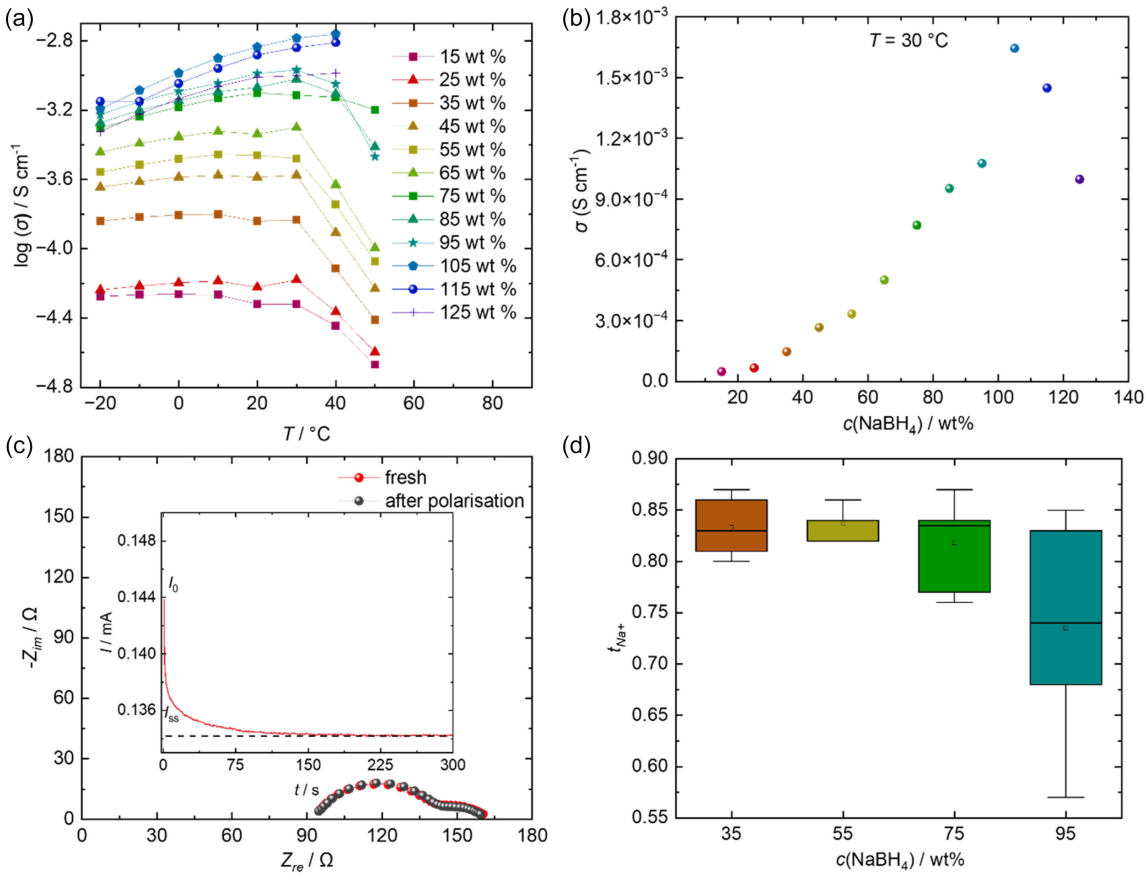

FIGURE 2 | (a) Ionic conductivity (log(σ)) versus temperature for the GPE samples containing varying concentrations of $NaBH_4$. (b) σ versus the $c(NaBH_4)$ in the GPEs at $T = 30$ °C. (c) Nyquist plots for the representative symmetric Na|GPE-GF/D|Na cells ($c(NaBH_4) = 55$ wt%) before and after polarization to determine R_0 and R_{ss}, respectively, with the inset showing the chronoampermetry data. (d) Box chart for the data representing the statistical evaluation of the transference number from six different cells. The top and bottom whiskers represent the total spread of the data, the box represents the inter quartile range, the central line is the median, and the datapoint is the mean value.

for 35, 55, 75, and 95 wt% of $NaBH_4$ are 240, 94, 64, and 47 Ω, respectively. The clear pattern of decreasing bulk resistance is indicative of the increasing conductivity of the electrolyte combination. Additionally, a clear separation of semicircles for Nyquist plot with 35 wt% electrolyte is observed in Figure S11a. Poor conductivity of 35 wt% electrolyte can form resistive SEI giving rise to well separated time constants helping in separating the semicircles, which can be attributed to bulk resistance for higher time constant and lower for charge-transfer resistance. The current response is monitored over time until a steady state (until a rate of change in current reaches below 0.01 μA s^{-1}) is attained and the polarization is stopped, after which EIS is conducted again to determine the steady-state resistance (R_{ss}) of the cell (see Figure 2c). Having these values, t_{Na^+} is calculated using the following equation [53]:

$$t_{Na^+} = \frac{I_{ss}}{I_0}\frac{(\Delta V - I_0 R_0)}{(\Delta V - I_{ss} R_{ss})} \quad (1)$$

where I_{ss} is the steady-state current, I_0 denotes the initial current, R_0 and R_{ss} represent the resistance before and after polarization, and ΔV is the voltage amplitude applied for polarization. To also evaluate the repeatability, we determine t_{Na^+} in sextuplicate, allowing us to perform a statistical evaluation. The results demonstrate high t_{Na^+} in all GPEs (t_{Na^+} in the range of 0.57–0.87), while the sample with $c(NaBH_4) = 55$ wt% exhibits the smallest spread of t_{Na^+} values and the highest mean t_{Na^+} among the studied samples (see Figures 2d and S11). This consistent performance indicates repeatability and homogeneous gel formation and reliable conductivity. Therefore, we concentrate on the $c(NaBH_4) = 55$ wt% GPE system for further electrochemical studies. The mean transference number for $c(NaBH_4) = 55$ wt% is $t_{Na^+} \approx 0.84$, substantially surpassing most commercial liquid electrolytes. A high t_{Na^+} indicates that the majority of the charge in the electrolyte is carried by the Na^+ ions, implying that the electrolyte is better able to cope with the concentration gradient formed within the electrolyte in contact with the electrode during cell operation. The consistently high values and low statistical spread observed for the optimized composition indicate that Na^+ ions dominate charge transport in this gel electrolyte. This behavior supports our hypothesis of immobilized anionic boron species in the GPE network: (1) of borate species within the polymer network by the reaction of between the BH_4^- and the hydroxyl groups of the fluoropolymer, and (2) noncovalent charge-inverted hydrogen bonding interactions of unreacted BH_4^- with hydrogens in the fluoropolymer backbone (as evident from ^{11}B NMR and IR spectra in Figure 1). Hydrogens in the fluoropolymer network are strongly positively polarized due to the electronegativity of neighboring fluorine atoms, whereas the hydride atoms on BH_4^- are strongly negatively polarized bonding interactions.

Such (B—H···H—C) charge-inverted hydrogen bonding interactions can significantly reduce anion mobility compared to conventional dual-ion conducting electrolytes [48, 55, 56]. A high t_{Na^+} also implies that the risk of dendrite development is reduced, making the electrolyte well-suited for sodium battery applications [57]. In general, this GPE demonstrates excellent ionic conductivity and superior t_{Na^+} at room temperature when compared to other recently reported electrolytes for sodium batteries (see Table S2).

Multiplying t_{Na^+} with the ionic conductivity σ of the electrolyte ($c(NaBH_4) = 55$ wt%, $T = 30\,°C$) gives the partial conductivity due to Na^+ ions $\sigma_{Na^+} = 2.8 \times 10^{-4}$ S cm^{-1}.

2.3 | Evaluation in Na|GPE|Na and Na|GPE|NVP/C Cells

To verify the compatibility of the GPE with Na metal, we performed galvanostatic plating stripping experiments in symmetric Na|GPE|Na cells wherein, the GPE is prepared by soaking a GF separator in the electrolyte. This is compared with a symmetric Na||Na reference cell employing commercially available 1 M $NaPF_6$ in tretraethylene glycol dimethyl ether (TEGDME) as the electrolyte. We employ 1 M $NaPF_6$ in TEGDME as a reference liquid electrolyte for comparison with our GPE as it is well described in the literature as an electrolyte [58]. The cells with 1 M $NaPF_6$ in TEGDME liquid electrolyte show only a very low overpotential of 7 mV in comparison to 16 mV with the GPE electrolyte (Figure 3a). This minimal overpotential of the liquid electrolyte-based cell in comparison with the GPE-based cell is attributed to the higher ionic conductivity $\sigma = 2.6 \times 10^{-3}$ S cm^{-1} of the liquid electrolyte [59]. Both cells (GPE and liquid electrolyte reference) continue to operate without a significant increase in overpotential up to 750 cycles (see Figure 3a) and representative plating and stripping profiles of the 503rd and 504th cycle are shown in Figure 3b. However, when the cells are operated at 1 mA cm^{-2}, we observe a reduced stability, where the GPE-based cell operates for up to 260 cycles before breaking down, whereas the cell with 1 M $NaPF_6$ in TEGDME only operates for up to 20 cycles before shorting (Figure 3c). To characterize the cell for the SEI formed during cycling, the cell is opened after 10 cycles of charge–discharge and Na anode is studied with scanning electron microscopy (SEM), energy-dispersive X-ray spectroscopy (EDS), and X-ray photoelectron spectroscopy (XPS). EDS study reveals the presence of trace amount of fluorine being part of SEI (see Figure S17a). Upon further analysis with XPS, there is a peak around 687 eV of binding energy, which corresponds to covalently bonded fluorine coming from the fluoropolymer

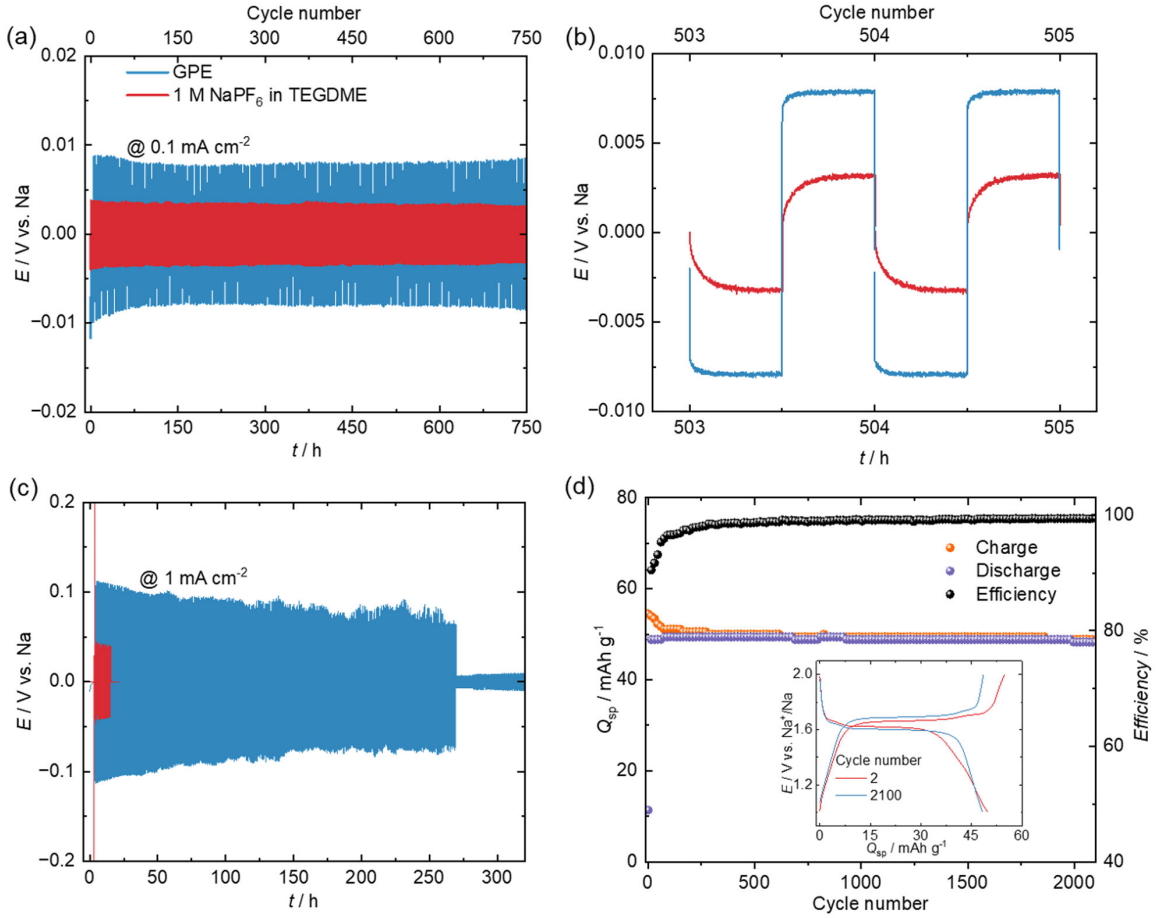

FIGURE 3 | (a) Comparative galvanostatic plating–stripping experiment for symmetric Na||Na cells with the GPE (blue) and 1 M $NaPF_6$ in TEGDME (red) as the electrolyte at 0.1 mA cm^{-2}. (b) Selected plating/stripping profiles for the 503rd and 504th cycle at 0.1 mA cm^{-2}. (c) Comparative galvanostatic plating–stripping experiment for symmetric Na||Na cells with the GPE (blue) and 1 M $NaPF_6$ in TEGDME (red) as the electrolyte at 1.0 mA cm^{-2}. (d) Long-term galvanostatic cycling of Na|GPE|NVP/C cells with $c(NaBH_4) = 55$ wt% for 2100 cycles; inset: selected discharge–charge profiles for the 2nd and 2100th cycle.

(see Figure S17c). Cycling stability study complemented with SEI composition study indicate that the GPE delays short-circuiting at elevated current densities compared to the liquid reference electrolyte, suggesting a more homogeneous Na plating/stripping behavior at the electrode | electrolyte interface formed by the fluoropolymer. In addition, we have also evaluated Na|GPE|Super P cell by carrying out cyclic voltammetry (CV) to verify suitability of the GPE in sodium metal battery application. Reversible plating (reduction) and stripping (oxidation) of Na on Super P is indicative that the GPE in the work is suitable for sodium-metal battery applications (see Figure S14b).

To finally evaluate also the potential use in practical cells, the compatibility with $Na_3V_2(PO_4)_3$/C (NVP/C) cathodes is studied in Na|GPE|NVP/C cells. NVP/C cathode shows 2 redox events corresponding to V^{4+}/V^{3+} and V^{3+}/V^{2+} at 3.4 and 1.6 V vs. Na respectively. We have chosen NVP/C cathode as we can access single electron redox event at 1.6 V. First, we conduct CV, revealing the characteristic redox couple centered around 1.6 V, which remains very stable for 10 consecutive cyclic sweeps, and is assigned to the V^{3+}/V^{2+} redox couple (see Figure S12) [60]. This stable cycling behavior prompts us to carry out long-term galvanostatic charge–discharge experiments. We access single electron V^{3+}/V^{2+} redox process for our study and hence the capacity is limited to 59 mAh g^{-1}. Accordingly, the cell with the GPE with $c(NaBH_4) = 55$ wt% at 1C (59 mA g^{-1}) shows an initial discharge capacity of 50 mAh g^{-1} and an initial Coulombic efficiency (CE) of 91% in the first cycle. Poor CE could be due to SEI formation and degradation of electrolyte in the initial cycles. Upon continuous cycling, the CE steadily improves and stabilizes at approximately 99.2%. The cell exhibits an overpotential of 91 mV in the 2nd cycle (see Figure S15c). Notably, the cell maintains stable cycling for more than 2100 cycles—the highest cycling stability among all GPE compositions investigated (see Figure S13)—while retaining 97% of its initial capacity (48 mAh g^{-1}) (see Figure 3d).

This excellent capacity retention indicates that only minimal side reactions of the electrolyte with the active cell components will occur, leading to the superior cell performance compared to the reference. By contrast, the reference cell with 1 M $NaPF_6$ in TEGDME electrolyte shows an initial discharge capacity of 52 mAh g^{-1} in the 2nd cycle, maintaining only 89% by the end of the 1600th cycle (see Figures S15).

3 | Conclusion

In this study, we design and synthesize a borate crosslinked Lumiflon fluoropolymer GPE. Experimental evidence confirms the formation of boron-centered crosslinks via the reaction of $NaBH_4$ and OH-groups in the fluoropolymer. The GPE shows maximum ionic conductivity at moderate $NaBH_4$ concentrations and around 30 °C, while higher concentrations or temperatures promote ion pairing and precipitation that hinder ion transport. The optimized GPE ($c(NaBH_4) = 55$ wt%) shows a reliable conductivity and consistent high transference number $t_{Na^+} \approx 0.84$. Finally, we demonstrate the compatibility and long-term cycling stability of the optimized GPE with SMB cells containing a Na-metal anode and NVP/C cathode, exhibiting stable cycling for more than 2100 cycles. While this study successfully demonstrates an efficient electrolyte system employing a commercially available fluoropolymer and cheap $NaBH_4$, further research should concentrate on enhancing the oxidative stability of this GPE system. Furthermore, this fluoropolymer-based electrolyte system can be extended to batteries using multivalent cations such as Mg^{2+}.

4 | Experimental Section

4.1 | Chemicals and Materials

Solvents and chemicals that we used for the preparation of the GPE are triethylene glycol dimethyl ether (TREGDME, ReagentPlus, 99%, Sigma–Aldrich), 1,2-dimethoxyethane (DME, anhydrous, 99.5%, Sigma–Aldrich), $NaBH_4$ (ReagentPlus, 99%, Sigma–Aldrich), PVDF (Sigma-Aldrich), SS316 CR2032 coin cell components (Shandong Gelon Lib Co. Ltd.), Super P (MTI Corp.), and 1 M $NaPF_6$ in tetraethylene glycol dimethyl ether (TEGDME, E-Lyte). The glass microfiber filter that we used was Whatman GF/D, Cytiva. All reagents that we used in the preparation of crosslinked films were used as received, except for TREGDME which was dried over molecular sieves and stored in an inert atmosphere.

4.2 | Basic Characterization of the Polymer

Fourier transform infrared spectroscopy (FTIR) was performed with a Perkin Elmer spectrometer, model Spectrum TWO. ^{11}B nuclear magnetic resonance (NMR) spectroscopy was conducted using the cross-polarization magic angle spinning (CPMAS) method on a Bruker AMX 400 spectrometer. The data analysis was carried out with the MestReNova software. The noncrystalline nature of the GPE was analyzed using X-ray powder diffraction (XRD, Stoe STADI P XRD diffractometer) in Debye–Scherrer geometry using a Mo Kα X-ray source 3 ($\lambda = 0.0709$ nm) at 50 kV, 40 mA. Diffraction patterns were recorded in a 2θ angle range between 5° and 70°.

4.3 | Ionic Conductivity

The ionic conductivity was determined using an automated Multiplexed Conductivity Meter, equipped with a frequency analyzer and a thermostatic chamber (MCS-10, MMates). The measurement involved using sealed glass conductivity cells equipped with two carbon coated platinum electrodes (see Figure S18). Prior to each measurement, the conductivity cells were calibrated, and their deviation constants were determined using the 0.01 M KCl in H_2O standard solution. The investigated electrolytes were then loaded into conductivity cells in a glovebox and sealed tightly. They were then allowed to stand at room temperature (3–4 days) for the gelation. The conductivity cells were then placed in a high temperature conductivity cell sample holder (HTCC) for the measurements. To ensure equilibrium, the samples were allowed to stabilize for 15 min before conducting the conductivity measurements. The conductivity of the electrolytes was measured in the frequency range from 50 kHz to 125 Hz by applying a perturbation of 10 mV. These measurements were carried out in the temperature range from −20 to 50 °C, with ramp steps of 10 °C.

4.4 | GPE-GF/D Preparation

A solution of fluoropolymer (110 mg) in 2.2 mL DME and 0.8 mL of 2 M $NaBH_4$ in TREGDME was mixed to make the electrolyte solution. Then 500 µL of the electrolyte solution was added into a vial containing the glass microfiber separator (GF/D) and it was allowed to stay for 3–4 days in an airtight container, allowing it to form the separator embedded with GPE cell (see Figure S10).

4.5 | NVP/C Cathode Preparation

The procured NVP/C cathode material had a carbon content of 9.8%. A mixture of NVP/C, conductive carbon Super P, and binder PVDF in the ratio of 8.5:1:0.5 ratio was ground thoroughly. The resulting mixture was transferred into a Thinky mixer capsule and a few drops of *N*-methyl-2-pyrrolidone solvent were added. The capsule was subjected to Thinky Mixer operation at 2000 rpm for 1 h to obtain smooth slurry. The resulting slurry was cast on battery-grade Al foil using the doctor blade technique and dried overnight. The coated foil was cut into circular electrodes with a diameter of 12 mm using a precision cutter.

4.6 | Coin Cell Fabrication

CR2032 coin cells were assembled inside a glove box maintained at <0.1 ppm for H_2O and O_2. To fabricate the cells with the GPE-impregnated GF/D as the electrolyte and separator, initially the NVP/C cathode was placed on the positive end plate, followed by GPE-GF/D, Na foil, spacer, spring, and negative end plate in the same order (see Figure S10). To fabricate the cells with 1 M $NaPF_6$ in TEGDME as the electrolyte, essentially the same procedure was employed, simply using GF/D as separator instead of the GPE-impregnated GF/D.

Acknowledgments

We thank AGC Chemicals Europe for providing a Lumiflon LF9716 sample. We thank Dr. Anna Smith from KIT for supplying us with the NVP/C sample. We sincerely thank Dr. Diego Ciardi, Dr. Davide Campagna, and Prof. Dr. Andreas Walther from the Department of Chemistry at Mainz University for discussions regarding the gel formation and rheology of the systems. We also thank Dr. Philipp A. Schuster from Ulm University for the help with DSC measurements. We thank the German Research Foundation (DFG) for funding within the priority program SPP 2248 Polymer-based Batteries and the POLiS Cluster of Excellence. This work contributes to the research performed at CELEST (Center for Electrochemical Energy Storage Ulm-Karlsruhe). L.J. and C.M. acknowledge the Alexander von Humboldt Foundation for postdoctoral fellowships.

Open Access funding enabled and organized by Projekt DEAL.

Funding

This study was supported by the Deutsche Forschungsgemeinschaft (DFG, German Research Foundation) funding numbers: 445470598, 445471097, 445471845, 441209207, and 390874152, and the Alexander von Humboldt-Stiftung.

Conflicts of Interest

The authors declare no conflicts of interest.

Data Availability Statement

The data that support the findings of this study are available from the corresponding author upon reasonable request.

References

1. C. Delmas, "Sodium and Sodium-Ion Batteries: 50 Years of Research," *Advanced Energy Materials* 8 (2018): 1703137.

2. J. Y. Hwang, S. T. Myung, and Y. K. Sun, "Sodium-Ion Batteries: Present and Future," *Chemical Society Reviews* 46 (2017): 3529–3614.

3. Y. Zhao, K. R. Adair, and X. Sun, "Recent Developments and Insights into the Understanding of Na Metal Anodes for Na-Metal Batteries," *Energy & Environmental Science* 11 (2018): 2673.

4. S. Lee, D. Kang, D. Y. Hyeon, et al., "Stable Sodium-Metal Batteries with a Hierarchical Structured Electrode toward Reversible Confinement of Na Dendrites," *Energy Storage Materials* 64 (2024): 103047.

5. Y. Wang, H. Yang, J. Xu, et al., "Competitive Coordination of Sodium Ions for High-Voltage Sodium Metal Batteries with Fast Reaction Speed," *Journal of the American Chemical Society* 146 (2024): 7332–7340.

6. C. Zhu, D. Wu, Z. Wang, et al., "Optimizing NaF-Rich Solid Electrolyte Interphase for Stabilizing Sodium Metal Batteries by Electrolyte Additive," *Advanced Functional Materials* 34 (2024): 2214195.

7. Y. Liu, Y. H. Zhang, J. Ma, J. Zhao, X. Li, and G. Cui, "Challenges and Strategies toward Practical Application of Layered Transition Metal Oxide Cathodes for Sodium-Ion Batteries," *Chemistry of Materials* 36 (2024): 54–73.

8. H. Darjazi, M. Falco, F. Colò, et al., "Electrolytes for Sodium Ion Batteries: The Current Transition from Liquid to Solid and Hybrid Systems," *Advanced Materials* 36 (2024): 2313572.

9. A. Basile, M. Hilder, F. Makhlooghiazad, et al., "Ionic Liquids and Organic Ionic Plastic Crystals: Advanced Electrolytes for Safer High Performance Sodium Energy Storage Technologies," *Advanced Energy Materials* 8 (2018): 1703491.

10. X. Wang, C. Zhang, M. Sawczyk, et al., "Ultra-Stable All-Solid-State Sodium Metal Batteries Enabled by Perfluoropolyether-Based Electrolytes," *Nature Materials* 21 (2022): 1057–1065.

11. L. Fan, S. Wei, S. Li, Q. Li, and Y. Lu, "Recent Progress of the Solid-State Electrolytes for High-Energy Metal-Based Batteries," *Advanced Energy Materials* 8 (2018): 1702657.

12. W. Hou, X. Guo, X. Shen, K. Amine, H. Yu, and J. Lu, "Solid Electrolytes and Interfaces in All-Solid-State Sodium Batteries: Progress and Perspective," *Nano Energy* 52 (2018): 279–291.

13. M. Yang, F. Feng, Z. Shi, J. Guo, R. Wang, and Z. Xu, "Facile Design of Asymmetric Flame-Retardant Gel Polymer Electrolyte with Excellent Interfacial Stability for Sodium Metal Batteries," *Energy Storage Materials* 56 (2023): 611–620.

14. D. Lei, Y. B. He, H. Huang, et al., "Cross-Linked Beta Alumina Nanowires with Compact Gel Polymer Electrolyte Coating for Ultra-Stable Sodium Metal Battery," *Nature Communications* 10 (2019): 4244.

15. C. Gao, X. Li, G. Wei, S. Wang, X. Zhao, and F. Kong, "Cellulose Acetate Propionate Incorporated PVDF-HFP Based Polymer Electrolyte Membrane for Lithium Batteries," *Composites Communications* 33 (2022): 101226.

16. D. Zhou, D. Shanmukaraj, A. Tkacheva, M. Armand, and G. Wang, "Polymer Electrolytes for Lithium-Based Batteries: Advances and Prospects," *Chem* 9 (2019): 2326–2352.

17. Q. Zhou, J. Ma, S. Dong, X. Li, and G. Cui, "Intermolecular Chemistry in Solid Polymer Electrolytes for High-Energy-Density Lithium Batteries," *Advanced Materials* 31 (2019): 1902029.

18. Q. Sun, S. Wang, Y. Ma, et al., "Fumaronitrile-Fixed In-Situ Gel Polymer Electrolyte Balancing High Safety and Superior Electrochemical

Performance for Li Metal Batteries," *Energy Storage Materials* 44 (2022): 537–546.

19. P. Xu, H. Chen, X. Zhou, and H. H. Xiang, "Gel Polymer Electrolyte Based on PVDF-HFP Matrix Composited with rGO-PEG-NH2 for High-Performance Lithium Ion Battery," *Journal of Membrane Science* 617 (2021): 118660.

20. Q. Wang, X. He, Y. Wang, et al., "In-Situ Constructing Efficient Gel Polymer Electrolyte with Fluoride-Rich Interface Enabling High-Capacity, Long-Cycling Sodium Metal Batteries," *Electrochimica Acta* 465 (2023): 142968.

21. H. Lai, Y. Lu, W. Zha, et al., "In Situ Generated Composite Gel Polymer Electrolyte with Crosslinking Structure for Dendrite-Free and High-Performance Sodium Metal Batteries," *Energy Storage Materials* 54 (2023): 478–487.

22. Z. Zhang, Y. Huang, C. Li, and X. Li, "Metal–Organic Framework-Supported Poly(ethylene Oxide) Composite Gel Polymer Electrolytes for High-Performance Lithium/Sodium Metal Batteries," *ACS Applied Materials & Interfaces* 13 (2021): 37262–37272.

23. H. Gao, B. Guo, J. Song, K. Park, and J. B. Goodenough, "A Composite Gel–Polymer/Glass–Fiber Electrolyte for Sodium-Ion Batteries," *Advanced Energy Materials* 5 (2015): 1402235.

24. M. Yang, F. Feng, Y. Ren, et al., "Coupling Anion-Capturer with Polymer Chains in Fireproof Gel Polymer Electrolyte Enables Dendrite-Free Sodium Metal Batteries," *Advanced Functional Materials* 33 (2023): 2305383.

25. X. Liu, X. Zheng, Y. Dai, et al., "Fluoride-Rich Solid-Electrolyte-Interface Enabling Stable Sodium Metal Batteries in High-Safe Electrolytes," *Advanced Functional Materials* 31 (2021): 2103522.

26. M. Xu, Y. Li, M. Ihsan-Ul-Haq, et al., "NaF-Rich Solid Electrolyte Interphase for Dendrite-Free Sodium Metal Batteries," *Energy Storage Materials* 44 (2022): 477–486.

27. S. Lin, Z. Yang, J. Chen, Y. Qiao, L. Li, and S. Chou, "Functional Electrolyte Additives for Sodium-Ion and Sodium-Metal Batteries: Progress and Perspectives," *Advanced Functional Materials* 34 (2024): 2400731.

28. W. Mo, S. Hu, H. Li, X. Zhu, and L. Zhang, "Designing Multifunctional Artificial SEI Layers for Long-Term Stability of Sodium Metal Anodes," *Journal of Colloid and Interface Science* 683 (2025): 600–609.

29. M. L. Lehmann, G. Yang, D. Gilmer, et al., "Tailored Crosslinking of Poly(ethylene Oxide) Enables Mechanical Robustness and Improved Sodium-Ion Conductivity," *Energy Storage Materials* 21 (2019): 85–96.

30. Y. Kang, K. Cheong, K. A. Noh, C. Lee, and D. Y. Seung, "A Study of Cross-Linked PEO Gel Polymer Electrolytes Using Bisphenol a Ethoxylate Diacrylate: Ionic Conductivity and Mechanical Properties," *Journal of Power Sources* 119–121 (2003): 432–437.

31. L. Ma, X. Li, J. Tan, et al., "Anion-Immobilized Gel Polymer Electrolyte with a High Ion Transference Number for High-Performance Lithium/Sodium Metal Batteries," *ACS Applied Materials & Interfaces* 15 (2023): 57201–57210.

32. Y. Li, F. Wu, Y. Li, et al., "Ether-Based Electrolytes for Sodium Ion Batteries," *Chemical Society Reviews* 51 (2022): 4484–4536.

33. C. Wang, A. C. Thenuwara, J. Luo, et al., "Extending the Low-Temperature Operation of Sodium Metal Batteries Combining Linear and Cyclic ether-Based Electrolyte Solutions," *Nature Communications* 13 (2022): 4934.

34. A. Ponrouch, E. Marchante, M. Courty, J. M. Tarascon, and M. R. Palacin, "In Search of an Optimized Electrolyte for Na-Ion Batteries," *Energy & Environmental Science* 5 (2012): 8572–8583.

35. Y. Lin, Q. Peng, L. Chen, et al., "Organic Liquid Electrolytes in Sodium-Based Batteries: Actualities and Perspectives," *Energy Storage Materials* 67 (2024): 103211.

36. D. Di Lecce, L. Minnetti, D. Polidoro, V. Marangon, and J. Hassoun, "Triglyme-Based Electrolyte for Sodium-Ion and Sodium-Sulfur Batteries," *Ionics* 25 (2019): 3129–3141.

37. X. Hou, T. Li, Y. Qiu, et al., "Interfacial Chemistry of Perfluorinated-Anion Additives Deciphering Ether-Based Electrolytes for Sodium-Ion Batteries," *ACS Energy Letters* 9 (2024): 461–467.

38. Q. Yu, Y. Xiao, S. Zhao, et al., "All-Fluorinated Low-Solvation Electrolytes for High-Voltage Sodium Metal Batteries with Appealing Stability," *Advanced Functional Materials* 34 (2024): 2401868.

39. X. Fan, X. Ji, L. Chen, et al., "All-Temperature Batteries Enabled by Fluorinated Electrolytes with Non-Polar Solvents," *Nature Energy* 4 (2019): 882–890.

40. C. V. Amanchukwu, Z. Yu, X. Kong, J. Qin, Y. Cui, and Z. Bao, "A New Class of Ionically Conducting Fluorinated Ether Electrolytes with High Electrochemical Stability," *Journal of the American Chemical Society* 142 (2020): 7393–7403.

41. Z. Yu, H. Wang, X. Kong, et al., "Molecular Design for Electrolyte Solvents Enabling Energy-Dense and Long-Cycling Lithium Metal Batteries," *Nature Energy* 5 (2020): 526–533.

42. X. Luo, A. Rawal, and K. F. Aguey-Zinsou, "Evidence of Superionic Na^+ Conductivity in Partially Hydrolyzed $NaBH_4$," *Journal of Physical Chemistry C* 128 (2024): 14861–14870.

43. J. Cuan, Y. Zhou, T. Zhou, et al., "Borohydride-Scaffolded Li/Na/Mg Fast Ionic Conductors for Promising Solid-State Electrolytes," *Advanced Materials* 31 (2019): 1803533.

44. F. Lu, Y. Pang, M. Zhu, et al., "A High-Performance Li–B–H Electrolyte for All-Solid-State Li Batteries," *Advanced Functional Materials* 29 (2019): 1809219.

45. W. Zhou, C. Song, S. Li, et al., "Low-Cost Preparation of High-Performance Na-B-H-S Electrolyte for All-Solid-State Sodium-Ion Batteries," *Advanced Science* 10 (2023): 2302618.

46. G. Eaton and W. Lipscomb, *NMR Studies of Boron Hydrides and Related Compounds* (W. A. Benjamin, 1969): 581–617.

47. S. Bulut, P. Klose, and I. Krossing, "Na[B(hfip)4] (hfip = OC(H)(CF3)2): A Weakly Coordinating Anion Salt and Its First Application to Prepare Ionic Liquids," *Dalton Transactions* 40 (2011): 8114.

48. Y. Konishi, H. Kokubo, S. Tsuzuki, R. Tatara, and K. Dokko, "A Partially Fluorinated Polymer Network Enhances the Li-Ion Transference Number of Sulfolane-Based Highly Concentrated Electrolytes," *Chemical Communications* 60 (2024): 12896–12899.

49. J. W. Suen, N. K. Elumalai, S. Debnath, et al., "Investigating the Correlation between Electrolyte Concentration and Electrochemical Properties of Ionogels," *Molecules* 28 (2023): 5192.

50. Z. Osman, M. M. Ghazali, L. Othman, and K. M. Isa, "AC Ionic Conductivity and DC Polarization Method of Lithium Ion Transport in PMMA–LiBF4 Gel Polymer Electrolytes," *Results in Physics* 2 (2012): 1–4.

51. C. F. Riadigos, R. Iglesias, M. A. Rivas, and T. P. Iglesias, "Permittivity and Density of the Systems (Monoglyme, Diglyme, Triglyme, or Tetraglyme +n-Heptane) at Several Temperatures," *Journal of Chemical Thermodynamics* 43 (2011): 275–283.

52. J. V. Kanth and H. C. Brown, "Improved Procedures for the Generation of Diborane from Sodium Borohydride and Boron Trifluoride," *Inorganic Chemistry* 39 (2000): 1795–1802.

53. J. Evans, C. A. Vincent, and P. G. Bruce, "Electrochemical Measurement of Transference Numbers in Polymer Electrolytes," *Polymer* 28 (1987): 2324–2328.

54. M. Forsyth, H. Yoon, F. Chen, et al., "Novel Na^+ Ion Diffusion Mechanism in Mixed Organic–Inorganic Ionic Liquid Electrolyte Leading to High Na^+ Transference Number and Stable, High Rate Electrochemical Cycling of Sodium Cells.," *Journal of Physical Chemistry C* 120 (2016): 4276–4286.

55. Y. Ma, S. Xu, X. Guo, et al., "Anion-Trapping Induced Solvation Optimization for High-Performance Polyester-Based Quasi-Solid-State Lithium Metal Batteries," *Advanced Functional Materials* 36 (2025): 16507.

56. V. Gupta, K. Singh, M. D. Singh, K. S. Nalwa, S. Narayanan, and R. Sarkar, "Designing Fluorocarbon-Based Polymeric Electrolytes with High Cationic Transference Number for All-Solid-State Sodium-Ion Batteries," *Polymer* 340 (2025): 129210.

57. J. Yu, M. Li, X. Kong, et al., "Polyanion Hydrogel Electrolyte with a High Zn^{2+} Transference Number for Dendrite-Free Aqueous Zinc-Ion Batteries," *Journal of Materials Chemistry A* 13 (2025): 16182–16192.

58. R. H. DeBlock, C. H. Lai, D. M. Butts, and B. S. Dunn, "Sodium-Ion Conducting Pseudosolid Electrolyte for Energy-Dense, Sodium-Metal Batteries," *Journal of Power Sources* 554 (2023): 232305.

59. Z. W. Seh, J. Sun, Y. Sun, and Y. Cui, "A Highly Reversible Room-Temperature Sodium Metal Anode," *ACS Central Science* 1 (2015): 449–455.

60. Z. Jian, L. Zhao, H. Pan, et al., "Carbon Coated $Na_3V_2(PO_4)_3$ as Novel Electrode Material for Sodium Ion Batteries," *Electrochemistry Communications* 14 (2012): 86–89.

Supporting Information

Additional supporting information can be found online in the Supporting Information section.